Korean J. Chem. Eng., 33(11), 3258-3266 (2016)
DOI: 10.1007/s11814-016-0159-6

pISSN: 0256-1115
eISSN: 1975-7220

Effects of modified LDPE on physico-mechanical properties of HDPE/$CaCO_3$ composites

Youngjun Ahn*, Jong Hyuk Jeon*, Ju-Hyoung Park, Thriveni Thenepalli***, Ji Whan Ahn***, and Choon Han*,†**

*Department of Chemical Engineering, Kwangwoon University, 20 Gwangun-ro, Nowon-gu, Seoul 01897, Korea
**Clean Fuel Laboratory, Korea Institute of Energy Research, 71-2, Jang-dong, Yuseong-gu, Daejeon 34129, Korea
***Mineral Resources Research Division, Korea Institute of Geoscience and Mineral Resources, 124 Gwahak-ro, Yuseong-gu, Daejeon 34132, Korea
(*Received 29 March 2016 • accepted 8 June 2016*)

Abstract−HDPE/$CaCO_3$/LDPE-g-MA composites of high density polyethylene (HDPE) and calcium carbonate ($CaCO_3$) with maleic anhydride grafted low density polyethylene (LDPE-g-MA) as a compatibilizer were prepared by melt mixing. LDPE-g-MA was prepared using a solution process. The maximum grafting degree was obtained at 6 wt% maleic anhydride (MA) and 0.2 wt% dicumyl peroxide (DCP) at 120 °C and 240 min. Functional groups not found in pure LDPE were observed with the formation of LDPE-g-MA. The successful dispersion of $CaCO_3$ particles in the HDPE matrix using LDPE-g-MA was revealed. The crystallite size of the composites was a little higher than that of $CaCO_3$. The mechanical properties of the HDPE/$CaCO_3$/LDPE-g-MA composites increased with decreasing $CaCO_3$ content. Thermogravimetric analysis (TGA) revealed a higher thermal stability for the HDPE/$CaCO_3$/LDPE-g-MA composites than for pure HDPE. Differential scanning calorimetry (DSC) revealed that the crystallization conditions were not substantially different. However, melting enthalpy and crystallinity increased with decreasing $CaCO_3$ content. The thermal stability was greatly improved compared to that previously reported for nano $CaCO_3$.

Keywords: Low Density Polyethylene, Maleic Anhydride, High Density Polyethylene, Calcium Carbonate, Polymer Composite

INTRODUCTION

Polymer/inorganic composites are hybrid materials composed of an organic polymer matrix with inorganic filler. Compared to pure polymers, the addition of inorganic fillers, such as talc [1], wollastonite [2], silica [3,4], TiO_2 [5], zirconium oxide [6], and calcium carbonate ($CaCO_3$) [2,7-14], improves the mechanical [11, 14] and thermal [2,15] properties due to the hybrid structure and interactions between the polymer and inorganic filler. However, due to the weak interfacial compatibility of hydrophobic polymers during mixing with hydrophilic inorganic particles, the mechanical properties of composites deteriorate with increasing inorganic filler content. As such, many studies have been conducted to enhance the interfacial compatibility between polymers and inorganic fillers. The Toyota Group has also performed extensive research on the development of nylon/clay composites with outstanding mechanical properties [16,17]. Cornell's Giannelis Group used tensile tests to study the toughening behavior of polyvinylidene fluoride (PVDF) reinforced with silicate particles [18].

Calcium carbonate ($CaCO_3$) is widely used in the plastic industry to enhance mechanical and thermal properties. Because of its rich deposits, low price, and variety of particle sizes, $CaCO_3$ is used as a filler in polyolefin composites. Many studies have found that mechanical, thermal, rheological, and morphological properties are influenced by $CaCO_3$ in a polyethylene (PE) matrix [11,19-21]. In the polymer matrix, $CaCO_3$ is difficult to disperse or stabilize due to its hydrophilic nature and large surface area. To enhance the dispersity of $CaCO_3$, modifying agents containing functional groups such as silane coupling agents, stearic acid, phosphate coupling agents, titanate coupling agents, and a surfactant are used [22-29]. However, the modified $CaCO_3$ exhibits weak interfacial bonding, due to the weak interfacial compatibility between macromolecular chains of the polymer matrix and molecules surrounding the $CaCO_3$ surface.

Among polyolefin polymers, PE is one of the most widely used. Some characteristics of PE include outstanding chemical resistance, strength, and processability [30,31]. It is difficult to disperse inorganic fillers in PE because the PE backbone is non-polar. Tanniru et al. [8] added $CaCO_3$ to high density polyethylene (HDPE) and found an increase in crystallinity and modulus, but a decrease in spherulite size arising from the nucleating effect. Lazzeri et al. [19] studied the mechanical and thermal properties of uncoated precipitated $CaCO_3$ (PCC) and coated PCC with stearic acid/HDPE composites, and showed a rapid decrease in Young's modulus and yield stress of coated PCC with the addition of stearic acid. Wang et al. [32] observed thermal degradation by mixing varying amounts of $CaCO_3$ with low density polyethylene (LDPE). Liang [33] showed that the melt flow rate of $CaCO_3$/LDPE/linear low density polyethylene (LLDPE) composites decreased with increasing $CaCO_3$

†To whom correspondence should be addressed.
E-mail: chan@kw.ac.kr

content. $CaCO_3$ was coated with stearic acid to enhance dispersion in the LDPE matrix and to the lower surface energy. The addition of stearic acid was associated with a higher modulus and yield stress, but lower tensile strength, yield strain, and ultimate elongation [34]. Moreover, the addition of nano-sized $CaCO_3$ in PE has been widely studied [19,35-39]. The mechanical and physical properties of PE/$CaCO_3$ composites improved when smaller particles of $CaCO_3$ were used [36]. However, the higher specific surface area caused more particle agglomeration [40]. Many studies focused on polymer/$CaCO_3$ nanocomposites, polymer/clay nanocomposites, and polymer/inorganic nanocomposites with modifying agents such as silane agents and stearic acid have examined mechanical, morphological, and thermal properties.

The purpose of this study was to analyze the novel behavior of HDPE/$CaCO_3$ composites with maleic anhydride grafted LDPE (LDPE-g-MA) as a compatibilizer. First, LDPE-g-MA was prepared using a solution process. LDPE modified with maleic anhydride (MA) was successfully added to HDPE/$CaCO_3$/LDPE-g-MA composites. The morphology, crystal structures and crystallite size of the HDPE/$CaCO_3$/LDPE-g-MA composites were compared, and the mechanical and thermal properties were also examined.

EXPERIMENTAL

1. Materials

HDPE (density 0.958 g/cm^3) and LDPE (density 0.921 g/cm^3) were obtained from LG Chemical Co., Korea. $CaCO_3$ (particle size ≈6.4 μm) was purchased from Duksan Co., Korea. Dicumyl peroxide (DCP, 98%), benzoyl peroxide (BPO, 75%), 2,2′-azobisisobutyronitrile (AIBN, 99%) as a radical initiator, and MA (98%) as a monomer were purchased from Sigma-Aldrich, USA. Xylene (80%) as a solvent and acetone (99.5%) as a washing agent for LDPE-g-MA were purchased from Daejung Chemical Co., Korea.

2. Preparation of LDPE-g-MA by Solution Process

LDPE-g-MA reactions were carried out by a solution process in a four-neck flask equipped with an impeller, thermocouple, and reflux condenser. In a typical experiment, 30 g of LDPE was dissolved in 300 mL of xylene at the desired temperature using a heating mantle. When LDPE was completely dissolved, the designated amount of MA was added. The designated amount of initiators that had been dissolved in 50 mL of xylene was then added to the reaction flask one by one. The reactions proceeded for 240 min, and samples were precipitated in 300 mL of acetone for 24 hours at room temperature. Next, samples were dried for 24 hours in a vacuum oven at 60 °C to remove non-reactive MA. To obtain the grafting degree of refined LDPE-g-MA, LDPE-g-MA was dissolved in 100 mL of xylene, and the solution was titrated until reaching the thymol blue end point using potassium hydroxide in ethanol (0.1 N). The grafting degree was calculated as follows:

$$\text{Acid number} = \frac{V_{KOH} \times N_{KOH} \times 56.1}{W_{gHDPE}} \quad (1)$$

$$\text{Grafting degree (\%)} = \frac{\text{Acid number} \times 98}{2 \times 561} \quad (2)$$

where V_{KOH} and N_{KOH} represent the volume (mL) used up in potassium hydroxide in ethanol and the equivalent concentration (0.1 N), respectively. W_{gLDPE} is 0.3 g of LDPE-g-MA.

Table 1. Description of the HDPE/$CaCO_3$/LDPE-g-MA composites

Sample name	Weight ratio (%) of HDPE/$CaCO_3$/LDPE-g-MA
HCLM1	1/9/2
HCLM2	2/8/2
HCLM3	3/7/2
HCLM4	4/6/2
HCLM5	5/5/2
HCLM6	6/4/2
HCLM7	7/3/2
HCLM8	8/2/2
HCLM9	9/1/2

3. Preparation of the HDPE/$CaCO_3$/LDPE-g-MA Composites

$CaCO_3$ was dried for eight hours in a vacuum oven at 80 °C to remove moisture before use. The surface treatment of $CaCO_3$ was not carried out, only $CaCO_3$ was physically mixed. Then, a fixed amount of LDPE-g-MA was melt mixed with varying ratio of HDPE and dried $CaCO_3$ (Table 1) in a Haake mixer (Rheomix 600, Germany) for five minutes at 180 °C at 50 rpm. The samples were then prepared by compression molding at constant pressure for two minutes at 130 °C using a hot press (Carver, USA). The sheet was cold pressed between two plates for three minutes at room temperature. A schematic diagram about making the LDPE-g-MA and HDPE/$CaCO_3$/LDPE-g-MA can be seen in Fig. 1.

4. Fourier Transform Infrared (FTIR)

FTIR spectra (JASCO, Japan) were used to verify the functional groups of pure LDPE and LDPE-g-MA. The attenuated total reflection (ATR) mode was used during measurement. The spectra comprised 80 scans and had a resolution of 2 cm^{-1} on average.

5. Scanning Electron Microscope (SEM)

All composites were coated with gold and were observed using SEM (SNE-3000M, Korea).

6. X-ray Diffraction (XRD)

XRD (Rigaku, Japan) was used to measure the dispersity of $CaCO_3$ in the composites. XRD patterns were collected at room temperature using Cu Kα radiation (λ=0.154 nm, 40 kV, 40 mA,

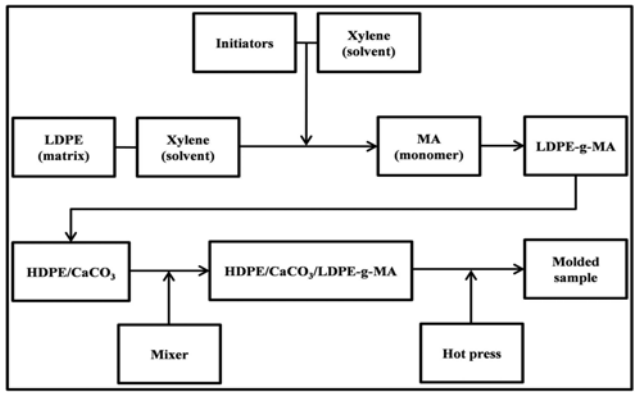

Fig. 1. Schematic diagram of LDPE-g-MA and HDPE/$CaCO_3$/LDPE-g-MA.

in the 2θ range from 10 to 50 degrees). Key patterns of HDPE and $CaCO_3$ were calculated under Bragg's law:

$$\lambda = 2d \sin\theta \quad (3)$$

where λ is the wavelength of the incident radiation, d is the interplanar spacing (nm), and θ is the scattering angle. Furthermore, the crystallite size of $CaCO_3$ and the HDPE/$CaCO_3$/LDPE-g-MA composites was evaluated from the Scherrer equation:

$$D = \frac{\kappa\lambda}{\beta\cos\theta} \quad (4)$$

where D is the crystallite size (nm), β is the full width half maximum (FWHM), θ is the scattering angle (°), the most common value for κ is 0.9 for FWHM of spherical crystal with cubic symmetry, the 0.154 nm as Cu Kα radiation has been widely used and then we applied these values.

7. Universal Testing Machine (UTM)

Tensile tests were performed on the composites at room temperature in accordance with ASTM D638. The mechanical properties of samples from HCLM1 to HCLM9 were measured with a UTM (Tinius Olsen, USA). A head speed of 10 mm/min was used for all cases, and the results of five tests were averaged.

8. Thermogravimetric Analysis (TGA)

TGA Q500 (TA instrument, USA) was used to determine the thermal stability of the composites. The specimens were heated at a rate of 5 °C/min from 25 °C to 900 °C in a nitrogen atmosphere.

9. Differential Scanning Calorimeter (DSC)

DSC Q1000 (TA instrument, USA) was used for differential scanning calorimetry. The composites were heated at a rate of 5 °C/min to 200 °C (first heating) and then cooled (second cooling) at a rate of 5 °C/min to ambient temperature in a nitrogen atmosphere. The crystallinity of the composites was calculated by the following:

$$X_C = \frac{\Delta H_C}{(1-\omega)\times\Delta H^*} \times 100 \quad (5)$$

where X_C is the crystallinity (%), ΔH_C is the measured melting enthalpy (J/g) from the first heating scan, ΔH^* is the melting enthalpy of HDPE (293 J/g) [41], and ω is the mass fraction of $CaCO_3$.

RESULTS AND DISCUSSION

1. Preparation of LDPE-g-MA

Fig. 2 shows the grafting degree in relation to MA content. The maximum grafting degree was 4.88% at 6 wt% MA and 0.2 wt% DCP at 120 °C. With increasing MA content, the grafting degree decreased. At high monomer content, a higher proportion of monomers are likely to be a higher proportion of monomers to attack the backbone. However, in reactions for LDPE-g-MA, the number of macroradicals was limited due to the influence of the initiator. Moreover, Sathe et al. [42] found that the addition of MA consumes radicals, which hastens the termination. For this reason, this study suggests that the polymer backbone can be influenced by adjusting the monomers content. The effect of the initiator

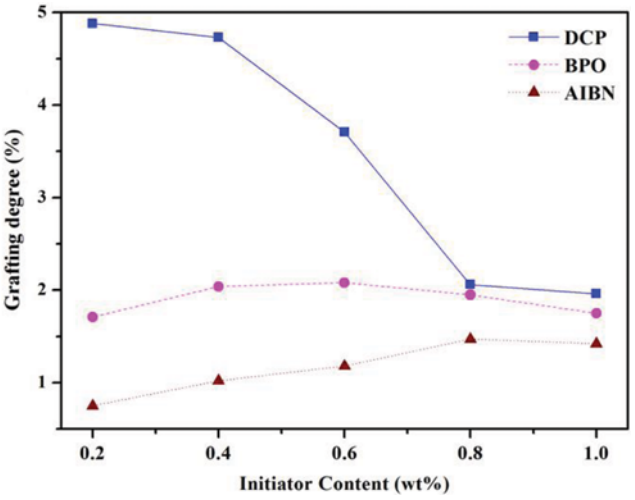

Fig. 3. The grafting degree of LDPE-g-MA with various initiators contents. Reaction conditions: 6 wt% MA, 120 °C, 240 min.

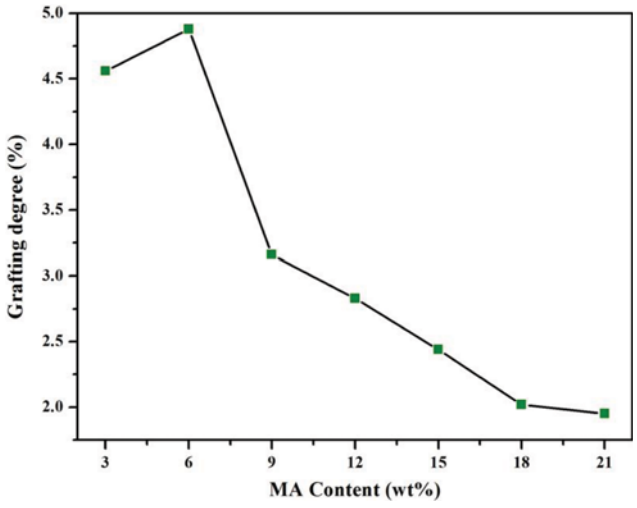

Fig. 2. The grafting degree of LDPE-g-MA with various MA contents. Reaction conditions: 0.2 wt% DCP, 120 °C, 240 min.

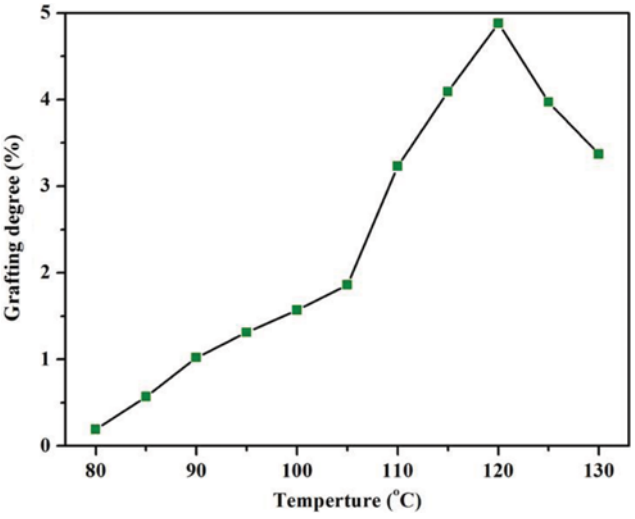

Fig. 4. The grafting degree of LDPE-g-MA with various temperature. Reaction conditions: 6 wt% MA, 0.2 wt% DCP, 240 min.

on the grafting degree is presented in Fig. 3. DCP, BPO, and AIBN as free radical initiators were used for LDPE-g-MA reactions at 120 °C. The grafting degree increased with increasing amounts of BPO and AIBN, but not for DCP. This can be traced to competitive reactions dependent on the amount of free radicals [43]. The half-life of initiators can be used as an indicator of the residual time in the reactant during grafting reactions. Initiators with shorter half-life undergo radical formation more quickly, and the recombination of radicals causes faster termination, thus decreasing the grafting degree [44]. Fig. 4 shows the effect of varying temperature at 6 wt% MA and 0.2 wt% DCP at 240 minutes. The grafting degree decreased at temperatures lower or higher than the reaction temperature of 120 °C. This coincides with studies on grafting degree at varying temperature by Shen et al. [45] and Ku Marsilla et al. [46]. The decrease in the grafting degree can be explained by the faster termination reaction because of the rapid decomposition of DCP at higher temperatures than 120 °C and the insufficient time for chain initiation due to the slow decomposition of DCP at lower temperatures than 120 °C. These results indicate that the highest grafting degree for LDPE-g-MA can be obtained at 120 °C and 240 min.

Fig. 5 shows the FTIR spectra of pure LDPE and LDPE-g-MA. The spectra of LDPE-g-MA show three peaks at 1,861 cm^{-1}, 1,790-1,780 (1,790, 1,784, 1,780) cm^{-1}, and 1,715 cm^{-1}, which were not found in pure LDPE. The peaks at 1,861 cm^{-1} and 1,790-1,780 cm^{-1} were from symmetric and asymmetric stretching of carbonyl in MA, while the peak at 1,715 cm^{-1} was from carbonyl stretching.

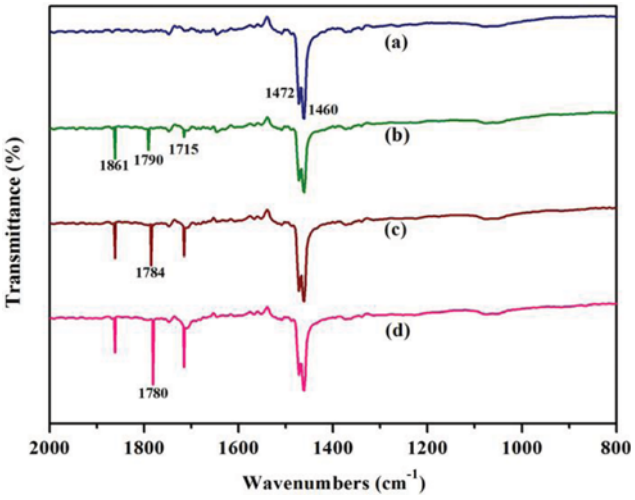

Fig. 5. FTIR spectra for (a) pure LDPE, (b) 1.95% grafting degree, (c) 2.83% grafting degree, and (d) 4.88% grafting degree. Reaction conditions: (b) 21 wt% MA, 120 °C, 240 min, (c) 12 wt% MA, 120 °C, 240 min, (d) 6 wt% MA, 120 °C, 240 min.

They are similar to the peaks of anhydride (1,861-1,750 cm^{-1}) and carboxylic acid (1,750-1,660 cm^{-1}) studied by Samay et al. [47]. Our goal in modified LDPE part was to check the tendency of grafting degree among various experimental conditions, and then we obtained the highest grafting degree from this tendency. We carefully proposed successful production because the LDPE-g-MA has

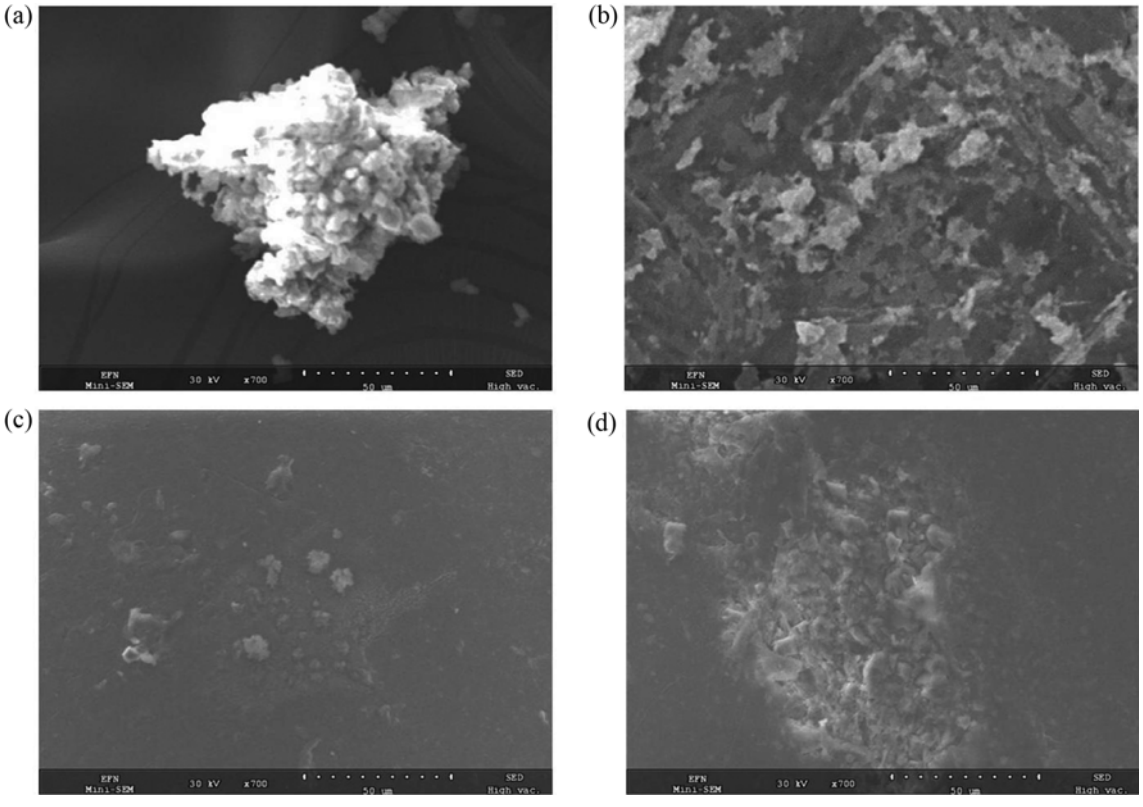

Fig. 6. SEM images of HDPE/$CaCO_3$ at weight ratios of (a) 1/9, (b) 2/8, (c) 8/2, and (d) 9/1 without LDPE-g-MA. Reaction conditions: Mixer 50 rpm, 180 °C, five minutes.

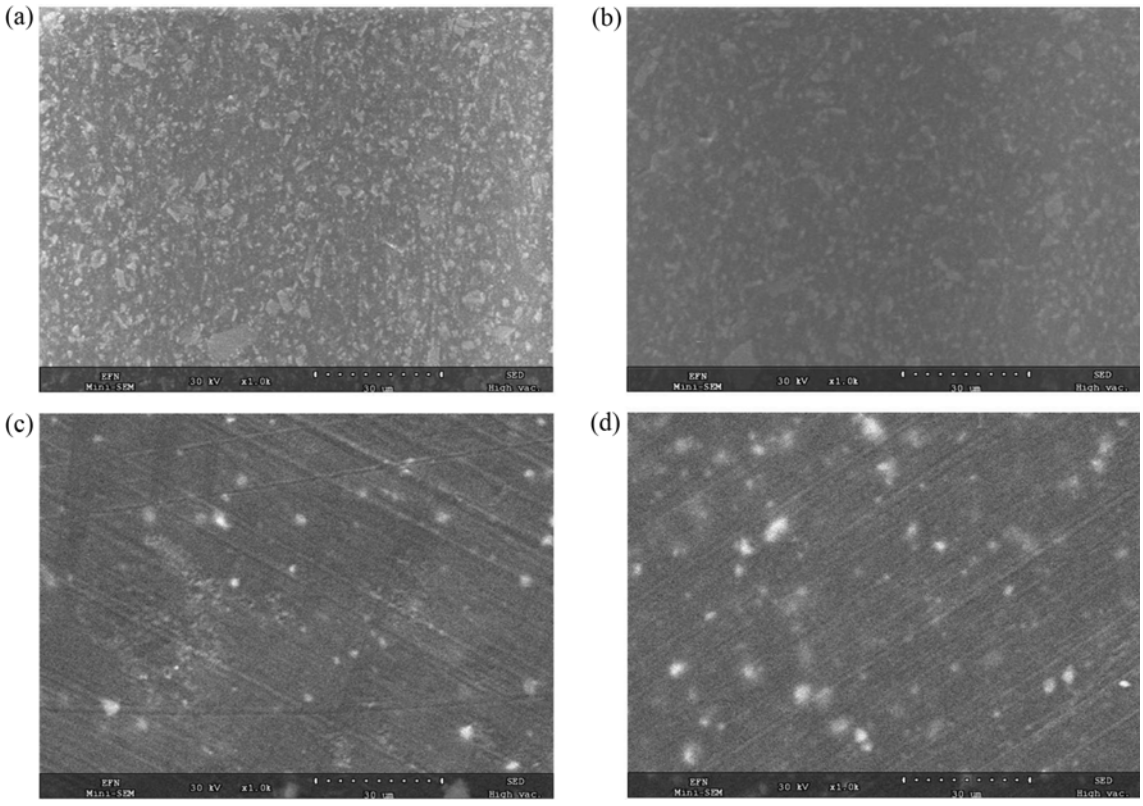

Fig. 7. SEM images of (a) HCLM1, (b) HCLM2, (c) HCLM8, and (d) HCLM9. Reaction conditions: Mixer 50 rpm, 180 °C, five minutes.

MA as monomer compared to pure LDPE.

2. Characterization of the HDPE/$CaCO_3$/LDPE-g-MA Composites

2-1. SEM Analysis

The SEM analysis of the HDPE/$CaCO_3$/LDPE-g-MA composites was performed to confirm the dispersion and aggregation of $CaCO_3$ particles in HDPE matrix. The dispersion of $CaCO_3$ particles in HDPE without LDPE-g-MA and HDPE with LDPE-g-MA is indicated in Figs. 6 and 7, respectively. The $CaCO_3$ particles in HDPE with LDPE-g-MA are regularly dispersed in the HDPE matrix and present relatively lower aggregation in Fig. 7. This result

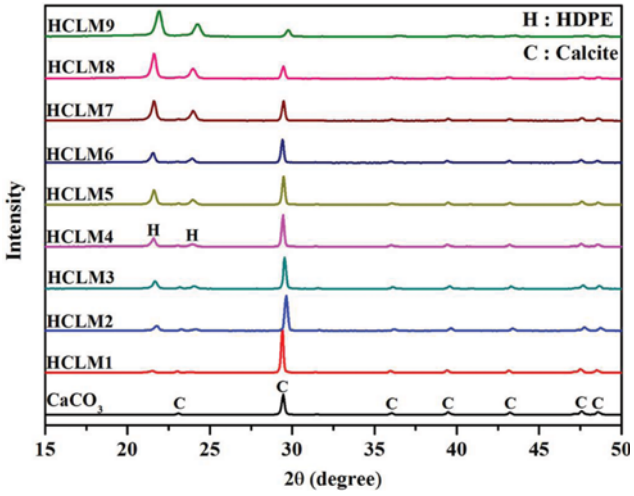

Fig. 8. XRD patterns of the HDPE/$CaCO_3$/LDPE-g-MA composites. Reaction conditions: Mixer 50 rpm, 180 °C, five minutes.

Table 2. Pattern positions of the HDPE/$CaCO_3$/LDPE-g-MA composites

Sample name	Angle (2θ)	d-Spacing (nm)	hkl
HDPE	22.55	0.394	(110)
$CaCO_3$	29.45	0.303	(104)
HCLM1	23.90	0.372	(110)
	29.40	0.303	(104)
HCLM2	23.30	0.381	(110)
	29.65	0.301	(104)
HCLM3	23.20	0.383	(110)
	29.55	0.302	(104)
HCLM4	23.05	0.385	(110)
	29.45	0.303	(104)
HCLM5	21.60	0.411	(110)
	29.45	0.303	(104)
HCLM6	21.55	0.412	(110)
	29.45	0.303	(104)
HCLM7	21.60	0.411	(110)
	29.50	0.302	(104)
HCLM8	21.6	0.411	(110)
	29.45	0.303	(104)
HCLM9	21.9	0.405	(110)
	29.75	0.300	(104)

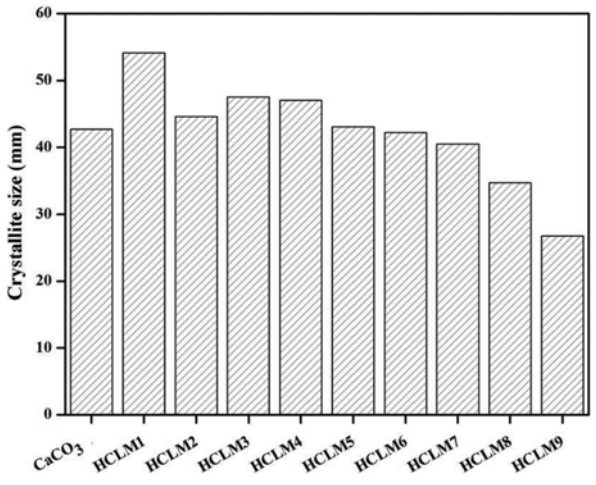

Fig. 9. Crystallite size of $CaCO_3$ and the HDPE/$CaCO_3$/LDPE-g-MA composites. Reaction conditions: Mixer 50 rpm, 180 °C, five minutes.

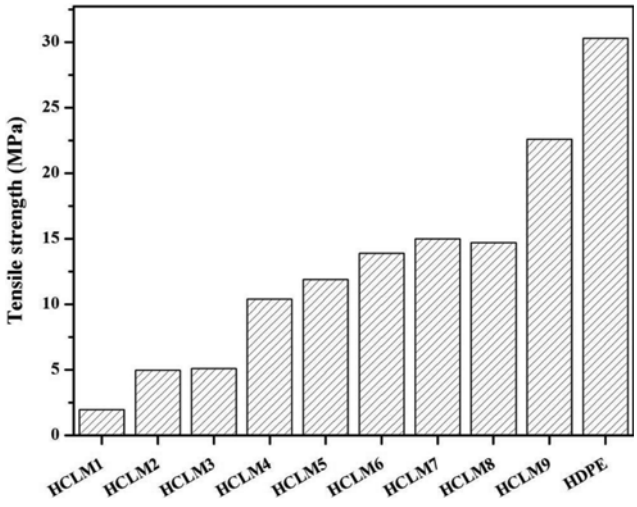

Fig. 10. Mechanical properties for the tensile strength of the HDPE/$CaCO_3$/LDPE-g-MA composites and pure HDPE. Reaction conditions: Mixer 50 rpm, 180 °C, five minutes.

indicates that LDPE-g-MA as a compatibilizer may improve interfacial interaction between the HDPE matrix and $CaCO_3$ particles.

2-2. XRD Analysis

Fig. 8 shows specific patterns, including calcite of $CaCO_3$, pure HDPE and HDPE/$CaCO_3$/LDPE-g-MA. Table 2 presents the scattering angles produced by specific patterns on $CaCO_3$ (104) and HDPE (110) planes. As shown in Fig. 8 and Table 2, the specific patterns of the HDPE/$CaCO_3$/LDPE-g-MA composites are similar to those of $CaCO_3$ and HDPE. The crystal structures of $CaCO_3$ and HDPE were not significantly different from that of the HDPE/$CaCO_3$/LDPE-g-MA composites. However, the crystallite size of HDPE/$CaCO_3$/LDPE-g-MA was determined from the FWHM of the strongest peak (104) using Eq. (4) in Fig. 9. Furthermore, we examined to focus the peak of $CaCO_3$ to check the presence of $CaCO_3$. The crystallite size mostly decreased with increasing $CaCO_3$ content, but crystallite size from HCLM1 to HCLM5 was a little higher than that of $CaCO_3$. This result indicates that the crystallite size of the HDPE/$CaCO_3$/LDPE-g-MA composites was probably affected by the LDPE-g-MA as a compatibilizer and LDPE-g-MA may help to improve the dispersion of $CaCO_3$. Furthermore, Fig. 8 shows that the intensity of the crystallinity of $CaCO_3$ and HDPE changes with additive amount. The higher intensity of HDPE is presumed to have been caused by the increased crystallinity, and this can be determined through DSC analysis.

2-3. UTM Analysis

Tensile properties provide useful information on the inner structure of composites [48]. The effect of $CaCO_3$ addition on the tensile strength of the HDPE/$CaCO_3$/LDPE-g-MA composites is shown in Fig. 10. The tensile strength of pure HDPE was similar to that of Chafidz et al. [49]. The tensile strength of the HDPE/$CaCO_3$/LDPE-g-MA composites increased with decreasing $CaCO_3$ content. The enhanced tensile strength of the composites can be traced to the improved dispersion with the small amount of filler in the polymer matrix. The tensile strength of composites is known to be influenced by the filler fraction and interaction or interfacial adhesion between the filler and polymer matrix. The load bearing capacity on the cross-sectional area of the HDPE/$CaCO_3$/LDPE-g-MA composites decreased with increasing $CaCO_3$ content despite the addition of LDPE-g-MA as a compatibilizer because of the weak interfacial compatibility between the HDPE matrix and $CaCO_3$. Similarly, the tensile strength of the HDPE/$CaCO_3$/LDPE-g-MA composites decreased with increasing $CaCO_3$ content, coinciding with a past study by Teixeira et al. [50]. We obtained a little higher tensile strength than the results of surface treatment of $CaCO_3$ [38]. These results suggest that tensile strength can be improved by focusing on $CaCO_3$ dispersion rather than on surface treatment of $CaCO_3$. The interfacial adhesion plays a key role in improving the tensile strength of composites. Composites with stronger interfacial adhesion are expected to induce greater stress and higher tensile strength.

2-4. TGA Analysis

Fig. 11 shows the TGA curves of pure HDPE and the HDPE/

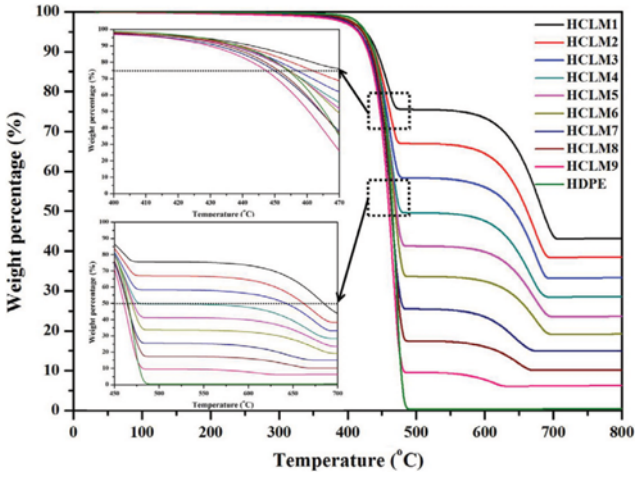

Fig. 11. TGA curves of the HDPE/$CaCO_3$/LDPE-g-MA composites and pure HDPE. Reaction conditions: Mixer 50 rpm, 180 °C, five minutes.

Table 3. Thermal stability conditions of the HDPE/$CaCO_3$/LDPE-g-MA composites under nitrogen atmosphere

Sample name	$T_{25\%}$ (°C)	$T_{50\%}$ (°C)	T_e (°C)
HDPE	465.20	465.20	485.29
HCLM1	562.68	684.35	705.13
HCLM2	461.53	661.69	689.28
HCLM3	456.76	641.96	687.27
HCLM4	454.21	477.79	685.66
HCLM5	453.97	471.27	681.24
HCLM6	454.34	469.35	664.37
HCLM7	449.62	464.09	660.05
HCLM8	449.55	464.03	659.99
HCLM9	447.10	460.42	628.86

Table 4. DSC conditions of crystallization for the HDPE/$CaCO_3$/LDPE-g-MA composites

Sample name	T_f (°C)	T_c (°C)	T_o (°C)	ΔH_c (J/g)	X_c (%)
HCLM1	123.48	126.03	138.32	21.21	28.96
HCLM2	123.71	126.94	139.3	40.20	41.15
HCLM3	123.81	128.58	141.25	81.32	66.59
HCLM4	123.65	129.65	142.23	104.00	70.99
HCLM5	126.13	128.74	138.81	125.70	73.53
HCLM6	122.97	130.53	143.69	153.30	78.47
HCLM7	123.70	128.76	140.27	180.10	81.96
HCLM8	125.01	131.82	144.67	212.10	86.86
HCLM9	125.22	129.62	139.78	229.70	85.51

$CaCO_3$/LDPE-g-MA composites. Table 3 presents the thermal stability conditions, such as the temperature at 25 wt% weight loss ($T_{25\%}$), temperature at 50wt% weight loss ($T_{50\%}$), and temperature at the end of degradation (T_e). The temperature of HDPE/$CaCO_3$/LDPE-g-MA at the end of degradation was higher than that of pure HDPE, and this temperature rose with increasing $CaCO_3$ content because of the $CaCO_3$ filler remaining in the composites. $T_{25\%}$, $T_{50\%}$, and T_e increased with increasing $CaCO_3$ content in the HDPE matrix, thereby enhancing the thermal stability of HDPE. This can be traced to $CaCO_3$ acting as a heat barrier in the thermal degradation process. The thermal stability was better than that previously reported for on nano $CaCO_3$ [51], implying that dispersibility is more important than the particle size of $CaCO_3$.

The thermal stability of the HDPE/$CaCO_3$/LDPE-g-MA composites showed regular changes because the melt mixing of LDPE-g-MA as a compatibilizer and $CaCO_3$ filler facilitated dispersion in the HDPE matrix.

2-5. DSC Analysis

The DSC curves of pure HDPE and the HDPE/$CaCO_3$/LDPE-g-MA composites at a cooling rate of 5 °C/min are shown in Fig. 12. Table 4 gives the crystallization onset temperature (T_o), crystallization temperature (T_c), crystallization finishing temperature (T_f), and crystallinity (X_c) of pure HDPE and HDPE/$CaCO_3$/LDPE-g-MA composites. The crystallinity of all composites was calculated using Eq. (5). T_c showed to the temperature of the maximum peak point of curves. T_f and T_o were to draw a baseline to curves, indicative of the temperature of both ends when the size of the area came out the same part. The T_f, T_c, and T_o of the composites were observed near 124 °C, 128 °C, and 140 °C, respectively. However, the melting enthalpy and crystallinity of all composites increased with decreasing $CaCO_3$ content. These results indicate that $CaCO_3$ has a little significant effect on the nucleation of the HDPE/$CaCO_3$/LDPE-g-MA composites. Fig. 12 shows an irregular shift of curves, indicating that $CaCO_3$ had a slight effect on nucleation in composites with LDPE-g-MA as a compatibilizer. This is similar to the findings of Bartczak et al. [52] on the crystallinity of $CaCO_3$ treated with calcium stearate. Furthermore, crystallinity from HCLM7 to HCLM9 was obtained higher than the previous results [25,52]. It was confirmed that $CaCO_3$ dispersed by LDPE-g-MA rather than $CaCO_3$ treated with calcium stearate [25], and stearic acid [52] was able to disperse polymer matrix. As shown above, the addition of $CaCO_3$ in the HDPE/$CaCO_3$/LDPE-g-MA composites exerted a minor influence on the nucleation.

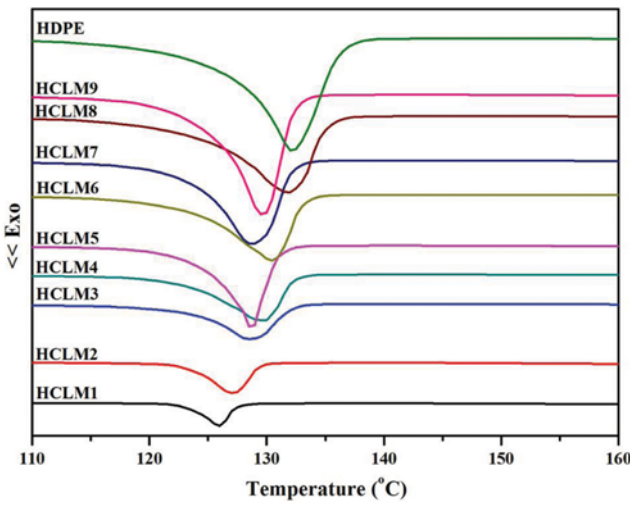

Fig. 12. DSC curves of the HDPE/$CaCO_3$/LDPE-g-MA composites and pure HDPE. Reaction conditions: Mixer 50 rpm, 180 °C, five minutes.

CONCLUSION

LDPE-g-MA was initially fabricated using a solution process. The maximum grafting degree was 4.88% with 6 wt% MA and 0.2 wt% DCP at 120 °C. The spectra of LDPE-g-MA showed three peaks that were not found in pure LDPE, and the peak intensity rose with increasing grafting degree. To maximize the grafting degree, specific conditions were required for DCP to interact with the LDPE matrix. HDPE/$CaCO_3$/LDPE-g-MA composites were produced using LDPE-g-MA with the highest grafting degree. The $CaCO_3$ particles in the HDPE matrix were successfully dispersed by using LDPE-g-MA as a compatibilizer, indicating that LDPE-g-MA plays a key role in dispersing $CaCO_3$ in the HDPE matrix. XRD patterns of the crystal structure showed no significant changes in pure HDPE, $CaCO_3$, and HDPE/$CaCO_3$/LDPE-g-MA composites. However, the crystallite size of the HDPE/$CaCO_3$/LDPE-g-MA com-

posites was a little larger than that of $CaCO_3$, suggesting that LDPE-g-MA as a compatibilizer may improve the dispersion of $CaCO_3$ in the HDPE matrix. Furthermore, the level of intensity was greatly influenced by the amount of HDPE and $CaCO_3$, which implies that $CaCO_3$ may be dispersed in the HDPE/$CaCO_3$/LDPE-g-MA composites through physical melt mixing instead of forming new materials via chemical reactions. The mechanical properties of the HDPE/$CaCO_3$/LDPE-g-MA composites deteriorated with increasing $CaCO_3$ content due to the minor interfacial compatibility between the HDPE matrix and $CaCO_3$, but the thermal stability improved with increasing $CaCO_3$. $T_{25\%}$, $T_{50\%}$, and T_e temperatures were higher for the HDPE/$CaCO_3$/LDPE-g-MA composites than for pure HDPE. This study also achieved better thermal stability than past research involving nano-$CaCO_3$ [51]. For the HDPE/$CaCO_3$/LDPE-g-MA composites, T_f, T_c, and T_o did not vary greatly in relation to DSC. However, the melting enthalpy and crystallinity increased with decreasing $CaCO_3$ content, coinciding with the results of past studies [52]. Based on the above, mechanical and thermal properties can be improved by focusing on $CaCO_3$ dispersion, rather than on $CaCO_3$ particle size, to enhance the interfacial compatibility. This composite may find application as a material for automotive weight reduction and filament of 3D printing.

ACKNOWLEDGEMENTS

The present research was conducted by the Korea Institute of Energy Technology Evaluation and Planning (Grant No. 2013T100100021) and the research grant of Kwangwoon University in 2016.

REFERENCES

1. R. S. Hadal and R. D. K. Misra, *Mater. Sci. Eng. A Struct. Mater.*, **374**, 374 (2004).
2. J. Z. Liang, B. Li and J. Q. Ruan, *Polym. Test.*, **42**, 185 (2015).
3. F. A. Santos and M. I. B. Tavares, *Polym. Test.*, **47**, 92 (2015).
4. L. Verdolotti, M. Lavorgna, R. Lamanna, E. D. Mail and S. Iannace, *Polymer*, **56**, 20 (2015).
5. F. S. Halek, S. K. Farahani and S. M. Hosseini, *Korean J. Chem. Eng.*, **33**, 629 (2016).
6. S. H. Lim, S. W. Seo, E. Jung, H. Chae and S. M. Cho, *Korean J. Chem. Eng.*, **33**, 1070 (2016).
7. C. M. Chan, J. Wu, J. X. Li and Y. K. Cheung, *Polymer*, **43**, 2981 (2002).
8. M. Tanniru and R. D. K. Misra, *Mater. Sci. Eng. A Struct. Mater.*, **405**, 178 (2005).
9. T. Tanniru and R. D. K. Misra, *Mater. Sci. Eng. A Struct. Mater.*, **424**, 53 (2006).
10. T. Thenepalli, A. Y. Jun, C. Han, C. Ramakrishna and J. W. Ahn, *Korean J. Chem. Eng.*, **32**, 1009 (2015).
11. H. Ghasemi, A. Mirzadeh, P. J. Bates and M. R. Kamal, *Polym. Test.*, **42**, 69 (2015).
12. J. Hu, Z. W. Wang, S. M. Yan, X. Q. Gao, C. Deng, J. Zhang and K. Z. Shen, *Polym.-Plast. Technol.*, **51**, 1127 (2012).
13. W. Y. Wang, X. F. Zeng, G. Q. Wang and J. F. Chen, *J. Appl. Polym. Sci.*, **106**, 1932 (2007).
14. T. Kato, *Adv. Mater.*, **12**, 1543 (2000).
15. A. Mirzadeh, H. Ghasemi, P. J. Bates and M. R. Kamal, *Int. Polym. Proc.*, **29**, 4 (2014).
16. W. Xu, M. Ge and P. He, *J. Appl. Polym. Sci.*, **82**, 2281 (2001).
17. W. B. Xu, S. P. Bao and P. S. He, *J. Appl. Polym. Sci.*, **84**, 842 (2002).
18. D. Shah, P. Maiti, E. Gunn, D. F. Schmidtt, D. D. Jiang, C. A. Batt and E. P. Giannelis, *Adv. Mater.*, **16**, 1173 (2004).
19. A. Lazzeri, S. M. Zebariad, M. Pracella, K. Cavalier and R. Rosa, *Polymer*, **46**, 827 (2005).
20. R. H. Elleithy, I. Ali, M. A. Ali and S. M. Al-Zahrani, *J. Appl. Polym. Sci.*, **117**, 2413 (2010).
21. S. Kwon, K. J. Kim, H. Kim, P. P. Kundu, T. J. Kim, Y. K. Lee, B. H. Lee and S. Choe, *Polymer*, **43**, 6901 (2002).
22. Z. Y. Yang, Y. J. Tang and J. H. Zhang, *Chalcogen. Lett.*, **10**, 131 (2013).
23. Z. Tang, G. Cheng, Y. Chen, X. Yu and H. Wang, *Adv. Powder Technol.*, **25**, 1618 (2014).
24. Z. S. Hu and Y. L. Deng, *Ind. Eng. Chem. Res.*, **49**, 5625 (2010).
25. İ. Özen and S. Şimşek, *Powder Technol.*, **270**, 320 (2015).
26. T. Nakatsuka, H. Kawasaki, K. Itadani and S. Yamashita, *J. Appl. Polym. Sci.*, **27**, 259 (1982).
27. R. Doufnoune, F. Chebira and N. Haddaoui, *Int. J. Polym. Mater.*, **52**, 967 (2003).
28. Z. G. Cui, Y. Z. Cui, C. F. Cui, Z. Chen and B. P. Binks, *Langmuir*, **26**, 12567 (2010).
29. L. Bao, S. Yang, X. Luo, J. Lei, Q. Cao and J. Wang, *Appl. Surf. Sci.*, **357**, 564 (2015).
30. G. Matsuba, S. Sakamoto, Y. Ogino, K. Nishida and T. Kanaya, *Macromolecules*, **40**, 7270 (2007).
31. A. Carbonell-Verdúa, D. García-Garcíaa, A. Jordáb, M. D. Sampera and R. Balarta, *Compos. Part B-Eng.*, **69**, 460 (2015).
32. W. Y. Wang, X. F. Zeng, G. Q. Wang and J. F. Chen, *J. Appl. Polym. Sci.*, **106**, 1932 (2007).
33. J. Z. Liang, *J. Appl. Polym. Sci.*, **104**, 1697 (2007).
34. M. A. Osman, A. Atallah and U. W. Suter, *Polymer*, **45**, 1177 (2004).
35. Q. Yuan, J. S. Shah, K. J. Bertrand and R. D. K. Misra, *Macromo Mater. Eng.*, **294**, 141 (2009).
36. S. Sahebian, S. M. Zebarjad and S. A. Sajjadi, *J. Thermoplast. Compos. Mater.*, **23**, 583 (2010).
37. A. Chafidz, I. Ail, M. E. A. Mohsin, R. Elleithy and S. Al-Zahrani, *J. Polym. Res.*, **19**, 9906 (2012).
38. H. U. Zaman, M. A. Khan, R. A. Khan and M. Dalour Hossen Beg, *J. Thermoplast. Compos. Mater.*, **27**, 1701 (2014).
39. J. Z. Liang and F. Wang, *Polym. Bull.*, **72**, 915 (2015).
40. A. Martinez-Garcia, A. Sanchez-Reche, C. M. Cepeda-Jimenez and J. M. Martin-Martinez, *Macromol. Symp.*, **221**, 23 (2005).
41. B. Wunderlich and M. Dole, *J. Polym. Sci.*, **24**, 201 (1957).
42. S. N. Sathe, G. S. Srinivasa Rao and S. Devi, *J. Appl. Polym. Sci.*, **53**, 239 (1994).
43. Z. Aimin and L. Chao, *Eur. Polym. J.*, **39**, 1291 (2003).
44. G. Moad, *Prog. Polym. Sci.*, **24**, 81 (1999).
45. Y. Shen, R. Qi, Q. Liu, Y. Wang, Y. Mao and J. Yu, *J. Appl. Polym. Sci.*, **110**, 2261 (2008).
46. K. I. Ku Marsilla and C. J. R. Verbeek, *Eur. Polym. J.*, **67**, 213 (2015).
47. G. Samay, T. Nagy and J. L. White, *J. Appl. Polym. Sci.*, **56**, 1423 (1995).

48. Y. Wang, X. Cao and L. Zhang, *Macromol. Biosci.*, **6**, 524 (2006).
49. A. Chafidz, I. Ali, M. E. A. Mohsiin, R. Elleithy and S. Al-Zahrani, *J. Polym. Res.*, **19**, 9860 (2012).
50. S. C. S. Teixeira, M. M. Moreira, A. P. Lima, L. S. Santos, B. M. Da Rocha, E. S. de Lima, R. A. A. F. da Costa, A. L. N. da Silva, M. C. G. Rocha and F. M. B. Countinho, *J. Appl. Polym. Sci.*, **101**, 2559 (2006).
51. S. Sahebian, S. M. Zebarjad and S. A. Sajjadi, *J. Thermoplast. Compos. Mater.*, **23**, 583 (2010).
52. Z. Bartczak, A. S. Argon, R. E. Cohen and M. Weinberg, *Polymer*, **40**, 2347 (1999).